Facile and efficient nitrogen modified porous carbon derived from sugarcane bagasse for CO2 capture: Experimental and DFT investigation of nitrogen atoms on carbon frameworks

Article · September 2019

DOI: 10.1016/j.cej.2019.122964

CITATIONS
0

READS
28

5 authors, including:

Omobayo Adio Salawu
King Fahd University of Petroleum and Minerals
11 PUBLICATIONS **79** CITATIONS
SEE PROFILE

Saheed Ganiyu
King Fahd University of Petroleum and Minerals
20 PUBLICATIONS **101** CITATIONS
SEE PROFILE

Muhammad Usman
King Fahd University of Petroleum and Minerals
27 PUBLICATIONS **258** CITATIONS
SEE PROFILE

Ismail Abdulazeez
King Fahd University of Petroleum and Minerals
14 PUBLICATIONS **50** CITATIONS
SEE PROFILE

Chemical Engineering Journal xxx (xxxx) xxxx

Contents lists available at ScienceDirect

Chemical Engineering Journal

journal homepage: www.elsevier.com/locate/cej

Facile and efficient nitrogen modified porous carbon derived from sugarcane bagasse for CO_2 capture: Experimental and DFT investigation of nitrogen atoms on carbon frameworks

Salawu Omobayo Adio[a], Saheed A. Ganiyu[a,b,*], Muhammad Usman[b,*], Ismail Abdulazeez[a], Khalid Alhooshani[a]

[a] Chemistry Department, King Fahd University of Petroleum & Minerals, 31261 Dhahran, Saudi Arabia
[b] Center of Excellence in Nanotechnology, King Fahd University of Petroleum & Minerals, 31261 Dhahran, Saudi Arabia

HIGHLIGHTS

- Highly porous nitrogen-doped carbon sorbent was synthesized via sustainable approach.
- CO_2-capture potential of nitrogen-doped carbon was superior to unmodified carbon.
- Increase in nitrogen amount and textural properties related to capturing efficiency.
- Nitrogen-doped carbon decreased the chemical hardness for efficient CO_2-capture.

GRAPHICAL ABSTRACT

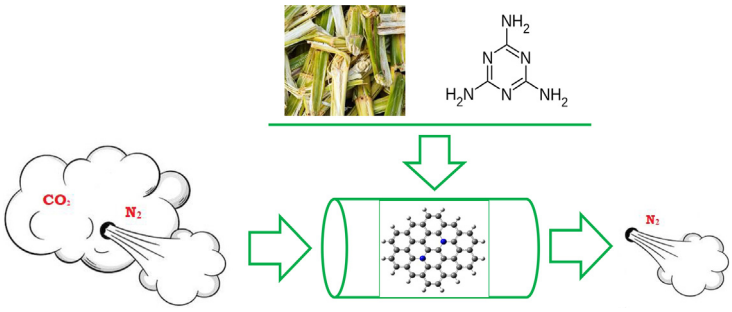

ARTICLE INFO

Keywords:
Sugarcane bagasse
Melamine
Nitrogen-doped carbon
CO_2-capture
DFT study

ABSTRACT

The use of sustainable feedstock and low-cost precursor is an important prerequisite in developing sorbents for CO_2 capture. In this research, nitrogen-modified porous carbon materials with varying ratio of carbon-melamine (1:1, 1:2 and 1:3) were synthesized from a sustainable and green-initiated feedstock, sugarcane bagasse, and solid-state impregnation of melamine and investigated as alternative sorbent in CO_2 capture. This gives an insight into the effect of increasing the nitrogen content of porous carbon material on CO_2 capture. The CO_2 uptake of the nitrogen-modified carbon was at least 35% more than that of the pristine porous carbon. Modified carbon with carbon-melamine ratio (1:2) demonstrates the highest CO_2 uptake at ambient pressure and temperature (3.34 mmol/g), making it comparable to similar materials that have been reported. The superiority demonstrated by this adsorbent was attributed to a balance between its textural properties and chemical functionalization using nitrogen. The synthesized material also showed high selectivity and regeneration capacities. Adsorption of CO_2 and N_2 on pristine and nitrogen modified carbon material was also examined using density functional theory (DFT) calculation at B3LYP/6-31G (d) level. The result obtained revealed that nitrogen-doped carbon material exhibited higher tendency to CO_2 adsorption than pristine carbon material in accordance with the hard-soft acid-base (HSAB) principle. This work provides a new and efficient route for the synthesis of nitrogen modified carbon and application for similar adsorption processes.

* Corresponding authors at: Chemistry Department, King Fahd University of Petroleum & Minerals, 31261 Dhahran, Saudi Arabia (S.A. Ganiyu).
E-mail addresses: gsadewale@kfupm.edu.sa (S.A. Ganiyu), muhammadu@kfupm.edu.sa (M. Usman).

https://doi.org/10.1016/j.cej.2019.122964
Received 20 June 2019; Received in revised form 23 September 2019; Accepted 24 September 2019

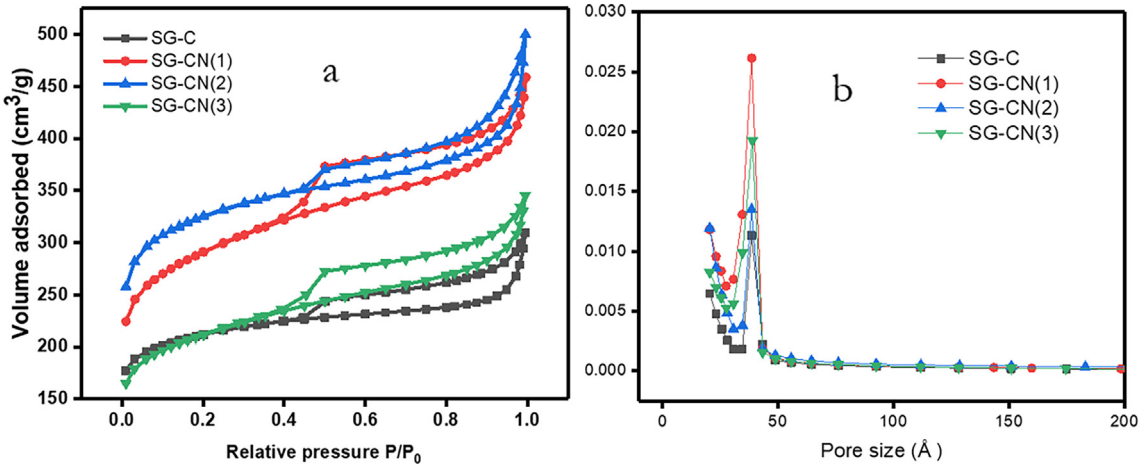

Fig. 1. (a) N_2 adsorption and desorption isotherms (b) Pore sizes of the parent carbon and synthesized SG-CN sorbents.

Table 1
BET Surface Properties of parent carbon and nitrogen-modified carbons.

Sorbent	BET Surface Area (m^2/g)	Micropore Area (m^2/g)	External Surface Area (m^2/g)	Total pore volume (cm^3/g)	Micropore volume (cm^3/g)	Average pore width (nm)	N-content by EDX (wt. %)
SG-C	684	454	230	0.41	0.23	5.92	–
SG-CN(1)	1000	542	458	0.64	0.25	4.86	2
SG-CN(2)	1111	717	395	0.67	0.33	6.02	3.4
SG-CN(3)	727	396	330	0.48	0.18	5.06	3.9

1. Introduction

Over the past few decades, carbon dioxide (CO_2) emission have been on the rise leading to a widespread concern since it is regarded as a major contributor to global warming. Since the industrial revolution, atmospheric CO_2 levels have increased by more than 39% [1]. Increase in atmospheric CO_2 concentration is directly influenced by the world's over dependence on fossil fuels to meet it continuous rise in energy demand [2,3]. CO_2 is a major greenhouse gas and causes climate change and global warming due to its capacity to absorb and emit radiation within the thermal infrared region [4]. As such, continuous increase in atmospheric CO_2 could be one of the major contributors to the increase in global surface temperature.

Different methods have been significantly researched to ensure carbon capture and hence reduce its emission to the atmosphere. These methods could be pre-combustion, post combustion or oxy-fuel combustion [5]. Post-combustion methods are more widely adopted due to their flexibility and the ease at which they can be combined with other technologies. Some of the post-combustion methods of CO_2 capture that have been used include but not limited to adsorption, chemical absorption, membrane separation and cryogenic separation.

Adsorption of CO_2 is regarded as a promising method due to the ease of operation and energy savings [6]. However, this technique is limited by the use of an appropriate sorbent. An efficient sorbent for CO_2 capture is expected to possess large specific surface area for adsorption, high selectivity, high regeneration ability and low energy demand for regeneration [1]. Different adsorbents have been used in CO_2 capture to meet these requirements including low temperature sorbents such as zeolitic materials [7–11], metal organic frameworks [12–14], activated carbon (AC) [15–18] intermediate temperature sorbents [19], and high temperature sorbents [20–22]. Carbon-based materials are often preferred as adsorbents due to their large-scale availability, porous structure, low cost, stability and high surface area [23].

Considering the widespread availability of carbon source such as bamboo, wood, coal, coconut husk etc., carbon-based materials have been regarded as a sustainable feedstock to produce novel adsorbents. Despite their tremendous properties, the use of carbon-based materials in catalysis, adsorption and other research areas is often limited. AC for instance, is limited by its poor selectivity while carbon nanotubes are often less dispersed in different media [24]. This limitation is sometimes removed by the incorporation of different desirable elements in carbon materials [25,26]. This provides a synergetic, novel material with the excellent surface properties of carbon and the desired chemical properties of the element added. Other sustainable feedstocks that have been used in synthesizing sorbents for CO_2 capture include coal-by products water treatment by products, biomass waste and household residues. As explained by Olivares-Marin et al., the efficiencies of these sorbents depends on the method of synthesis, properties of the precursor and the modifications on the adsorbents [27]. Recently, a number of studies have been reported on the modifications of carbon with different elements [28–31,18]. It has been demonstrated that introduction of different heteroatoms such as phosphorus, boron, oxygen and nitrogen change the surface and electronic properties of carbon materials [32,30]. Specifically, nitrogen modified carbon materials have shown improved catalytic properties and enhanced surface polarity. In a typical nitrogen modified carbon, nitrogen is alkaline and influences the spin density of surrounding carbon atoms [33]. In addition, the presence of nitrogen affects charge distribution on carbon atoms and provides electron donor properties to carbon [34]. This may explain the excellent adsorption of CO_2 on nitrogen modified carbon materials. The modification of carbon with nitrogen can be done by post-synthetic amine modification or ammonia treatment of oxidized carbon [35]. The latter is less preferred because of the use of corrosive reagents and the materials obtained from this procedure often lack stability. Nitrogen can also be added to a porous carbon framework using nitrogen containing precursors such as melamine and urea [36–38].

While it has been established that nitrogen enhances the adsorption of CO_2, very little is known on the effect of the increase in nitrogen content on the adsorption process. As such, herewith, the effect of increasing nitrogen content on CO_2 adsorption was investigated. Carbon

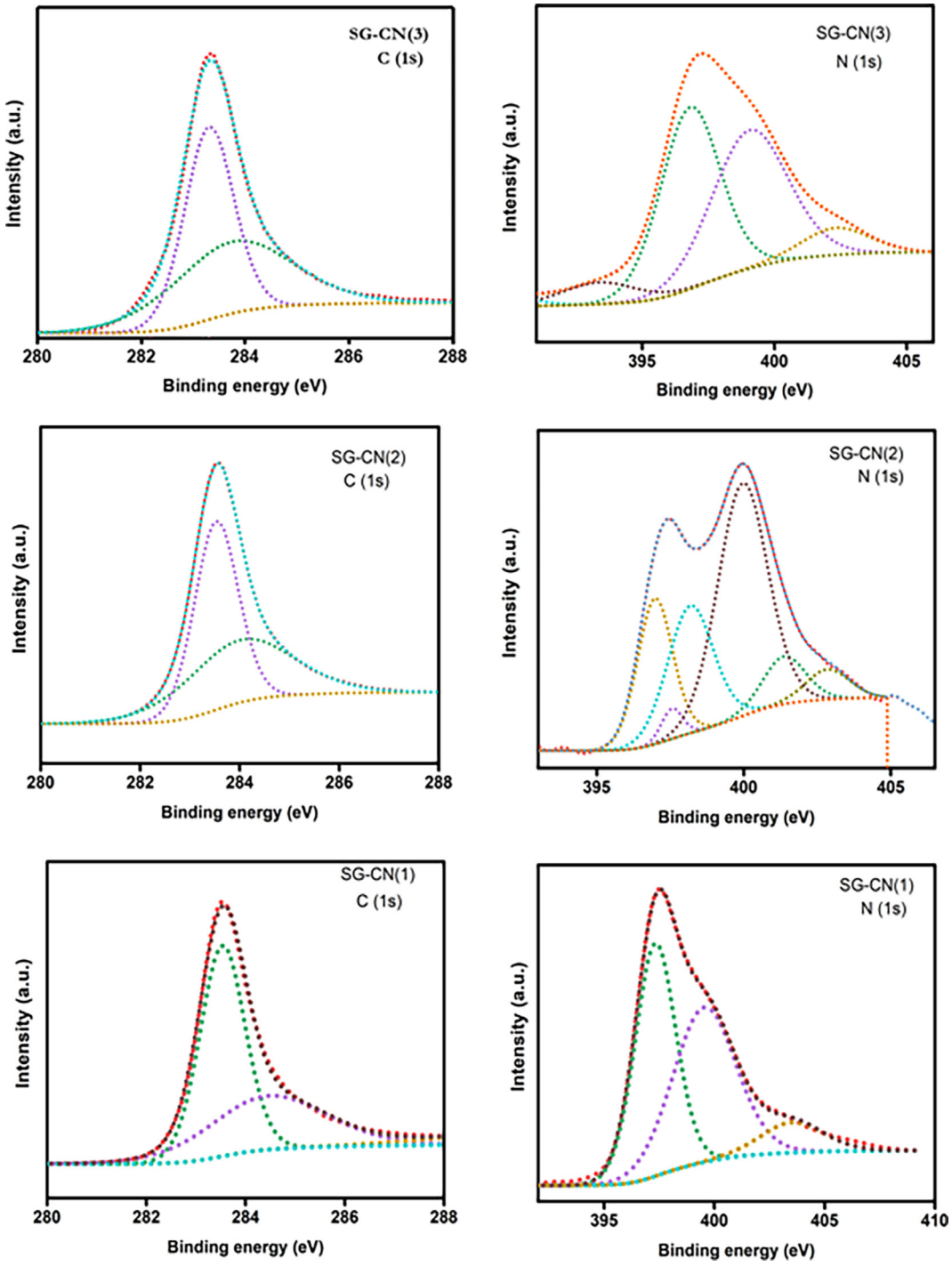

Fig. 2. XPS spectra of SG-CN sorbents.

was prepared using sugarcane bagasse as a feedstock and activated by wet impregnation. Melamine was subsequently used as a nitrogen rich source to modify the synthesized carbon material by solid state. The nitrogen to carbon content in the synthesized material was varied in different ratios to investigate the effect of increasing nitrogen modification and textural properties on CO_2 capture. Insights into the role of chemical hardness of the pristine carbon and nitrogen-modified carbon on CO_2 adsorption were evaluated using DFT studies. The nitrogen-doped carbon material exhibited lower HOMO/LUMO (highest-occupied/lowest-unoccupied molecular orbitals) energy gap, lower global hardness and resulted in higher tendency to CO_2 adsorption than pristine carbon material in accordance with the hard-soft acid-base (HSAB) principle.

2. Material and methods

2.1. Materials

All chemicals used were of analytical grade. Zinc-acetate and Melamine (> 99% purity) were obtained from Sigma Aldrich (India). Sugarcane bagasse was obtained from a farm in Hassanzai village, Shabqadar, KPK, Pakistan. The nitrogen gas used during the pyrolysis process was of ultra-high purity grade (UHP 99.9999%). All other chemicals used were also of ultra-high purity grade. High purity de-

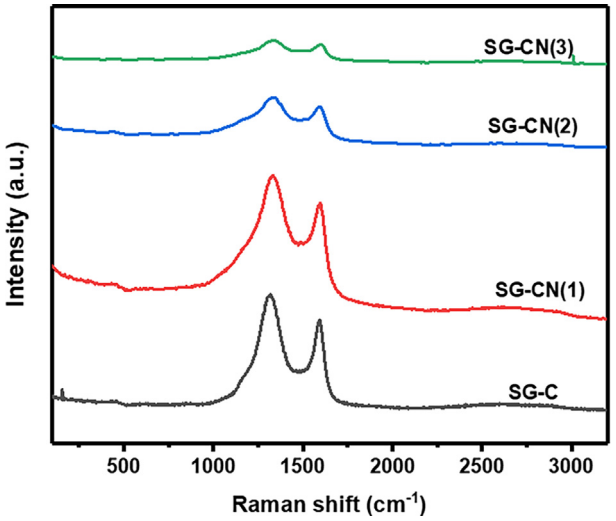

Fig. 3. Raman spectra of SG-C and SG-CN sorbents.

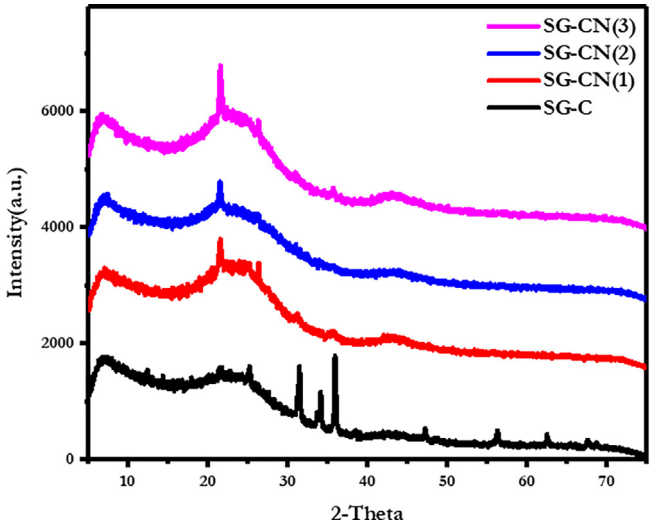

Fig. 4. XRD spectra of parent carbon and SG-CN sorbents.

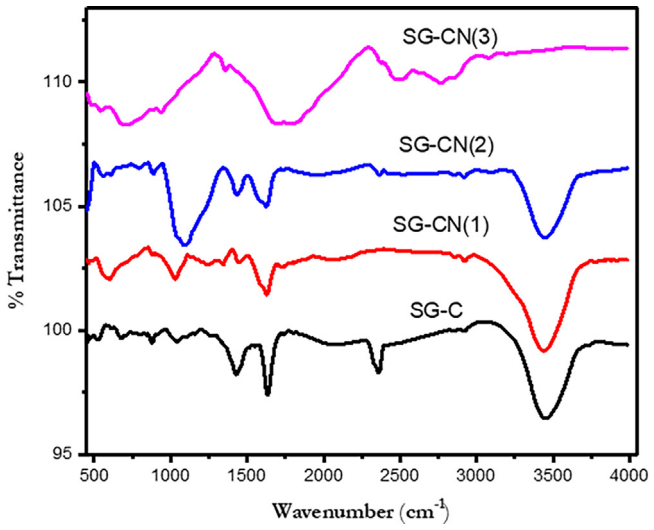

Fig. 5. Spectra obtained from FT-IR analysis of parent carbon and nitrogen-modified carbon sorbents.

ionized water (DI-H_2O) was produced in the laboratory and used throughout the experiment.

2.1.1. Synthesis of pristine porous carbon

Pristine porous carbon was synthesized by washing and drying sugarcane bagasse at 100 °C for 6 h. The dried bagasse was activated by wet impregnation using zinc acetate solution at a precursor-activator ration of 1:1. This was subsequently dried by slow evaporation at 60 °C. The sample was further dried at 100 °C for 6 h and pyrolyzed in 50 mm horizontal quartz tubular furnace at 900 °C for 60 min under the flow of high purity (99.999%) nitrogen gas. The sample was cooled to room temperature (RT) under the same inert environment to obtain porous and high surface area carbon material and denoted SG-C.

2.1.2. Synthesis of nitrogen modified porous carbon

The nitrogen modified porous carbon material was prepared from the pristine porous carbon described in 2.2.1 above. However, melamine was used as nitrogen source for the modification process. The modification process was carried out by solid state impregnation of the pristine porous carbon with melamine by varying the melamine content in the ratios 1:1, 1:2 and 1:3. The mixture was heat-treated at 900 °C in N_2-gas environment for 1 h to obtain the adsorbent. The samples were denoted SG-CN(1), SG-CN(2), SG-CN(3) with respect to carbon-melamine ratio (1:1, 1:2 and 1:3), respectively.

2.2. Surface characterization

Nitrogen sorption isotherms and textural properties of both the untreated and treated carbon materials were measured using N_2 adsorption method at −196 °C. This procedure was done according to the conventional volumetric technique using Micrometrics ASAP 2020 surface area and porosity analyzer. Binding energies of the materials were obtained using X-ray photoelectron spectroscope (PHI 5000 Versa Probe II, ULVAC-PHI Inc.) carried out with mini Al Kα radiation maintained under ultrahigh vacuum. Raman spectroscopy was used to measure the blue wavelength excitation to determine the carbon composition of the adsorbents. These measurements were taken at room temperature using NXR FT-Raman module spectrograph attached to an InGaAs detector. IR analyses of the adsorbent samples were measured by Fourier Transform Infrared spectrometer (Nicolet 6700 FT-IR, Thermo Electron Corporation). The instrument has a resolution of 2.0 cm^{-1}, an OMNIC program and a deuterated triglycine sulfate detector. Each sample was analyzed according to the potassium bromide (KBr) method. Each sample spectrum was recorded in transmission mode and at wavelength range 4000–500 cm^{-1}. Surface morphology of the sugarcane bagasse derived carbon (pristine) and that treated with melamine by impregnation was obtained using Field Emission Scanning Electron Microscope FESEM (TESCAN, LYRA 3) coupled with EDX for elemental analysis.

2.3. Experimental studies of CO_2 adsorption

The total adsorptions of CO_2 by the prepared samples were analyzed using Autosorb (Quant chrome). In a typical procedure, 100 mg of sample was taken in a tube and degassed at 120°C. The sample is ramped at 5 °C/min and held for 6 h after which it was cooled to 25°C. Subsequent doses of CO_2 were injected and each point of equilibrium recorded. The measurement was continued till 760 torr. A controlled vacuum was used to degas the sample and a plot was recorded based on the adsorption and desorption of CO_2. The same procedure was applied to measure the CO_2 uptake at 40°C. Nitrogen adsorption–desorption isotherm was also calculated using the same procedure. Isosteric heat of adsorption (Qst) for CO_2 was calculated from the adsorption isotherms while the selectivity of CO_2 compared to N_2 was calculated using single component isotherms by Henry's law.

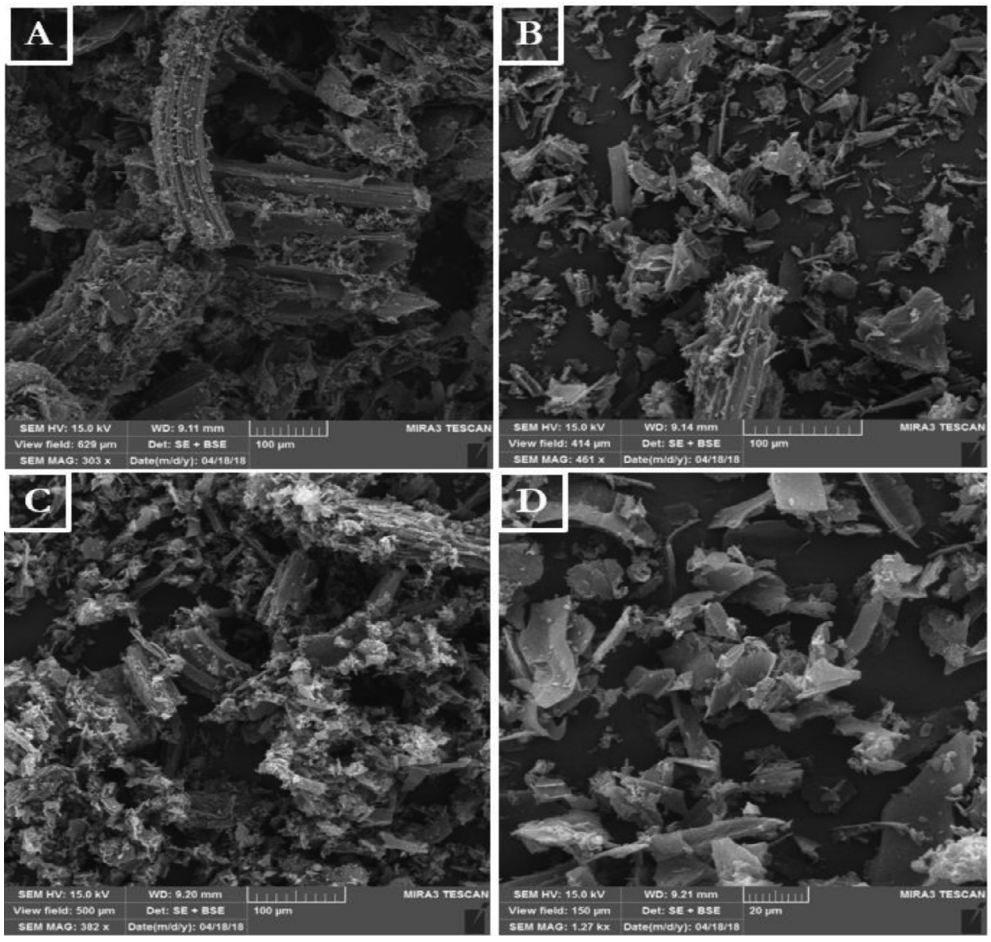

Fig. 6. SEM images of SG-C and SG-CN materials (A) SG-C, (B) SG-CN(1), (C) SG-CN(2) and (D) SG-CN(3).

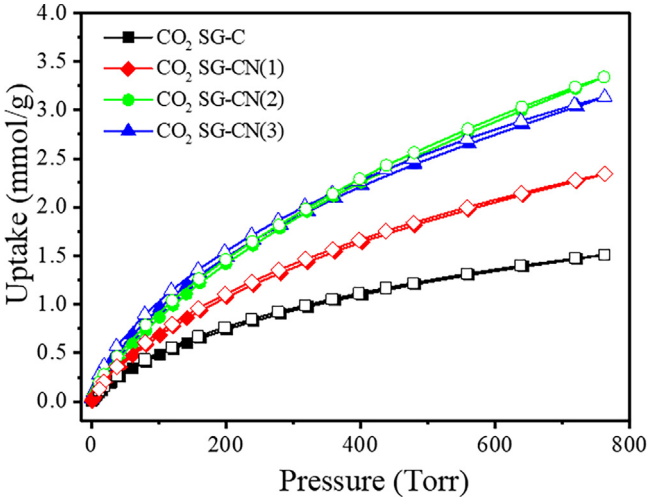

Fig. 7. CO_2 sorption isotherms at 298 K on biomass derived activated carbon and SG-CN sorbents.

Table 2
The BET surface area and CO_2 adsorption capacity of different prepared SG-CN materials at 298 K.

Sorbent	A_{BET}(m^2 g^{-1})	CO_2 uptake (mmolg^{-1})
SG-C	684	1.51
SG-CN(1)	1000	2.34
SG-CN(2)	1111	3.34
SG-CN(3)	727	3.13

2.4. Computational studies

The adsorption mechanisms were studied using theoretical calculations based on density functional theory (DFT). The parent sugar cane derived carbon material was represented by the coronene model while nitrogen modification was done by substituting two carbon atoms within the central coronene structure with nitrogen atom. The carbon material, modified carbon material, CO_2 and N_2 molecule were drawn using Gaussview software [39]. DFT calculations were carried out using Gaussian 09 package [40] to optimize the geometries of the interaction of modified and non-modified carbon with CO_2 and to evaluate the adsorption energy and hence binding tendencies between the adsorbents and CO_2. The calculation was also used to evaluate the selectivity of the adsorbents for CO_2 compared to N_2. Geometry optimizations and calculations involving frequencies and energies of studied molecules were done using Density Functional theory (DFT) with Becke 3-Parameter (Exchange), Lee, Yang and Parr. (B3LYP). The calculations were performed using 6-31 G (d) basis set.

3. Result and discussion

3.1. Surface characterization analysis

3.1.1. BET surface area analysis

The surface properties of the parent sugarcane derived carbon material (SG-C) and the different SG-CN samples were compared using N_2 adsorption and desorption isotherms (Fig. 1). The isotherm observed

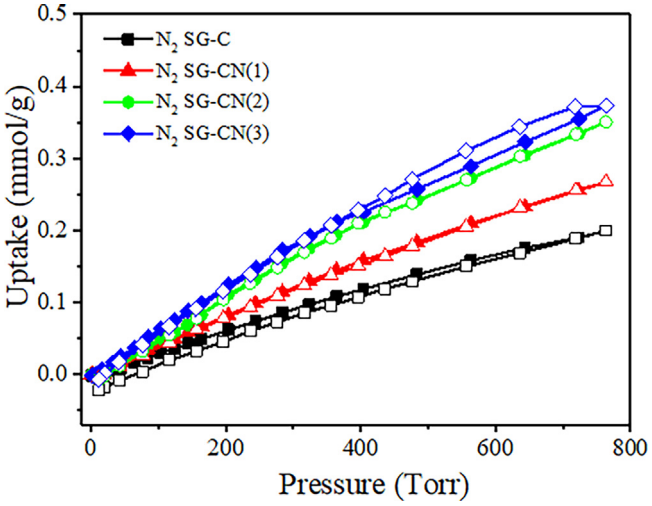

Fig. 8. N_2 sorption isotherms at 298 K on biomass derived activated carbon and SG-CN sorbents.

Table 3
Comparison of the CO_2 adsorption capacity of different materials.

Material	T(*K*)	P (bar)	CO_2 uptake (mmol g^{-1})	Refs.
MCM-41-NH_2	308	2.5	1.2	[69]
PS	313	1	3.63	[70]
A2-BPMO	298	1.2	3.03	[71]
Hierarchical porous CN spheres	298	1	2.90	[72]
a-MCN	298	1	2.69	[62]
P-g-C_3N_4	298	1	0.39	[73]
MCN/C	298	1	2.35	[74]
SG-CN(2)	298	1	3.34	This work

can be described as type IV in accordance with the IUPAC classification [41,42]. Type IV BET isotherm is used to describe adsorbents that have pore sizes ranging between 1.5 and 100 nm with a mixture of micropores and mesopores [43,44]. The adsorption nature in this type of isotherm is considered monolayer- multilayer with capillary condensation. Also, the slope in type IV isotherm is observed to experience an increased uptake of adsorbate as pores are filled, at higher pressures and inflection point are known to occur near completion of the first monolayer. H3 hysteresis loop was also observed in all the plots which can be attributed to the mesoporous nature of the adsorbents. Hysteresis loops occur due to the difference in filling and emptying of the mesopore mechanism by capillary condensation. A summary of the surface properties including the surface area, micropore volume and average pore width is also provided in Table 1. As shown, SG-CN(2) exhibited the highest BET surface area. Also, all the modified carbon materials have higher BET surface area compared to SG-C. It was observed that incorporation of melamine at lower nitrogen content (between 1:1 and 1:2) and further heat treatment increases the surface area of the sorbents. However, at higher melamine content, the surface area decreases despite same heat treatment. This can be inferred from the tendency of melamine to cause surface coverage at higher quantity, thereby decreasing the surface area. Therefore, the optimum loading of melamine on pristine carbon was found around (1:2 carbon-melamine ratio). The external surface area and micropores volume obtained from the DeBoer t-plot is also presented in Table 1. All the SG-CN samples were observed to have higher external surface area compared to the parent carbon sample. The pore sizes of the samples are shown in Fig. 1(b). All the samples have maximum pore size around 30 A. There is also similarity in the pore sizes of both the parent carbon material and the SG-CN samples.

3.1.2. XPS spectroscopy analysis

Further surface information and chemical state of C and N in the synthesized samples were obtained using XPS analysis (Fig. 2). The C 1 s spectrum of all the samples shows carbon species at a binding energy of around 283 eV. The C 1 s spectrum was further deconvoluted into three Gaussian-Lorenzian peaks to understand the chemical bonding between carbon and nitrogen atoms in the modified carbon samples. The four peaks obtained have binding energies; 283 eV, 284 e, 287 eV. The fitted C 1 s energy peak around 284 eV is assigned to pure graphitic sites in the amorphous CN matrix. The peak around 284 eV is assigned to graphitic C=C [45] while that observed at 287 eV corresponds to CN bonding in graphitic carbon nitride and nitrogen-doped carbon [46]. The N 1 s spectrum of SG-CN(1) and SG-CN (3) also shows four deconvoluted peaks at 397, 400, 401 and 404 eV. However, seven peaks were obtained for SG-CN(2). The peaks obtained at around 397 eV is attributed to sp^2 N atoms which could also be attributed to the fact that the sp^2 N atoms is surrounded by two carbon atoms [46]. The peaks at 400 eV is assigned to trigonal bonding of N atoms to sp^2 carbon atoms. It can also correspond to amorphous C-N network where N atoms are bounded to two sp^2 carbon atoms and one sp^3 carbon atom [47]. The surface characterization results obtained are consistent with those reported by previous literature in the synthesis of carbon nitride or nitrogen-modified carbon.

3.1.3. Raman spectroscopy analysis

Raman spectroscopy is used in the characterization of carbon materials to determine their microstructure. The two bands of a typical carbon and nitrogen-doped carbon spectrum were observed at approximately 1350 and 1580 cm^{-1} [48,49]. These two bands correspond

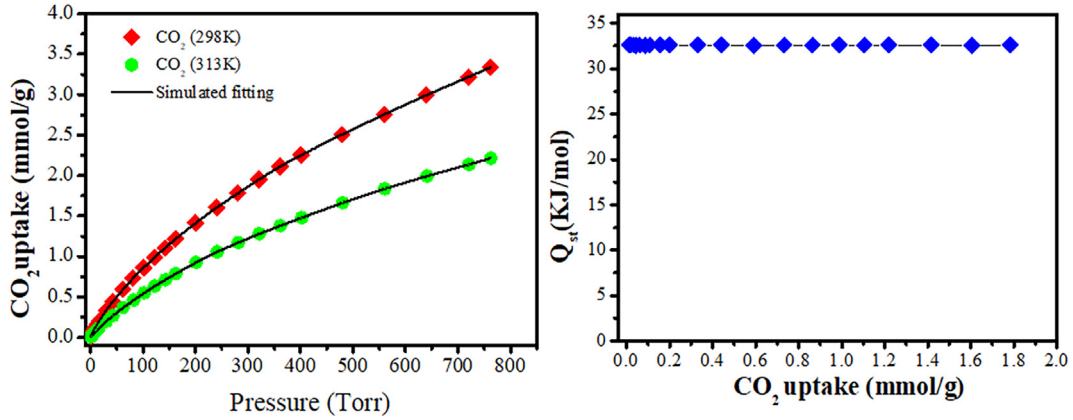

Fig. 9. Isosteric heat of adsorption (Qst) on SG-CN(2) versus CO_2 uptake shows the physisorption CO_2 interaction with the framework with 32.61 kJ mol^{-1}.

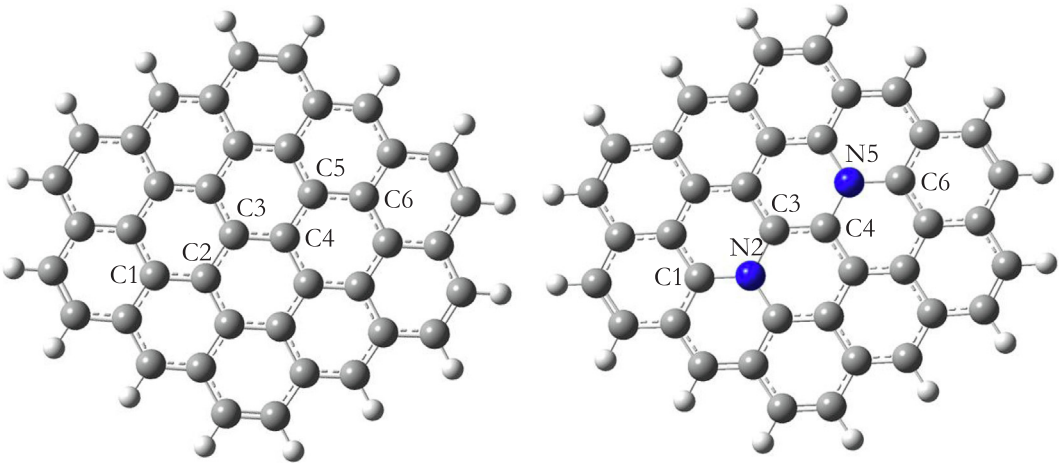

Fig. 10. Optimized structures of (a) coronene model that depicts pristine sugar cane derived carbon materials (b) nitrogen substituted coronene that depicts modified carbon material.

Table 4
Bond properties of selected atoms, binding distances and adsorption energies of CO_2 and N_2 on SG-C and SG-CN at B3LYP/6-31G(d).

Interaction	Bond	Bond distance (Å)	Angle	Bond Angle (°)	Binding distance (Å)	Adsorption energy (Kcal/mol)
Interaction of adsorbent with CO_2						
	C1-C2	1.421(1.421)	C1-C2-C3			
	C2-C3	1.429(1.429)	C2-C3-C4	120.0(120.0)		
SG-C/CO_2	C3-C4	1.412(1.412)	C3-C4-C5	120.0(120.0)	3.721	−48.92
	C4-C5	1.429(1.429)	C4-C5-C6	120.0(120.0)		
	C5-C6	1.421(1.421)		120.0(120.0)		
	C1-N2	1.402(1.403)	C1-N2-C3			
	N2-C3	1.411(1.413)	N2-C3-C4	119.8(119.8)		
SG-CN/CO_2	C3-C4	1.404(1.403)	C3-C4-N5	120.0(120.0)	3.243	−51.86
	C4-N5	1.413(1.413)	C4-N5-C6	120.0(120.0)		
	N5-C6	1.403(1.403)		119.8(119.8)		
Interaction of adsorbent with N_2						
	C1-C2	1.421(1.421)	C1-C2-C3			
	C2-C3	1.429(1.429)	C2-C3-C4	120.0(120.0)		
SG-C/N_2	C3-C4	1.412(1.412)	C3-C4-C5	120.0(120.0)	3.970	−34.22
	C4-C5	1.429(1.429)	C4-C5-C6	120.0(120.0)		
	C5-C6	1.421(1.421)		120.0(120.0)		
	C1-N2	1.403(1.403)				
	N2-C3	1.412(1.413)	C1-N2-C3	119.8(119.8)		
SG-CN/N_2	C3-C4	1.403(1.403)	N2-C3-C4	120.0(120.0)	3.637	−35.29
	C4-N5	1.413(1.413)	C3-C4-N5	120.0(120.0)		
	N5-C6	1.403(1.403)	C4-N5-C6	119.8(119.8)		

[a]Values in parenthesis represents bond distances in isolated AC, SO3H-AC and F-AC.
[b]Values in parenthesis represents bond angles in isolated AC, SO3H-AC and F-AC.

to the D and G bands of the Raman spectrum of amorphous graphitic carbon as shown in Fig. 3 [50]. The second order peak (less intense) usually observed in highly graphitic carbon between 2300 and 3000 cm^{-1} is broad and weak in all samples analyzed, indicating that the as-synthesized carbon and nitrogen-doped carbons are less graphitic [51]. It should be mentioned that the intensity of characteristic D and G-bands of nitrogen-doped porous carbon decreases with increasing nitrogen content (high melamine ratio), especially for SG-CN(2) and SG-CN(3). This observation might be correlated to an increase in disorderliness in the carbon matrix.

3.1.4. XRD analysis

The crystal structure of the parent carbon and modified carbon samples were characterized by XRD as shown in Fig. 4. Multiple peaks were obtained in the XRD spectrum of the parent carbon material obtained from sugarcane bagasse. Most of these peaks were absent in the synthesized SG-CN sorbents. The modified samples contain mainly two peaks at around 22° and 26° and are indexed as 100 and 002. The peak at around 26° can be attributed to stacking peak of π-conjugated layers [52–54].

3.1.5. FT-IR spectroscopy analysis

The functional groups present on the SG-CN samples were determined using FT-IR analysis as shown in Fig. 5. IR bands were observed around 3400 cm^{-1} and 2900 cm^{-1}. The band around 3400 can be attributed to the presence of N–H symmetric stretching vibrations [55]. This band has also been seen in terminal amino groups of graphitic carbon nitride [56]. The band around 2900 cm^{-1} corresponds to C–H stretching vibrations of $–CH_2$-NH-CH_2 or $–CH_2$-NH-CH_3 while those observed around 1600 and 1200 are attributed to plane deformation in N–H and C-N stretching vibrations respectively [57]. Bands that exists within these wavelengths, attributed to C-N heterocycle stretches as well as bands around 800 cm^{-1} have been reported in unmodified carbon nitrides [58]. Less intense bands around 900 and 600 cm^{-1} corresponds to deformation vibrations of out of plane N–H [59]. The IR bands observed corroborate the presence of N–H and C-N functional groups in the modified samples [60].

3.1.6. SEM analysis

The surface morphology of the samples was observed under scanning electron microscope (SEM). As shown in Fig. 6, all the samples

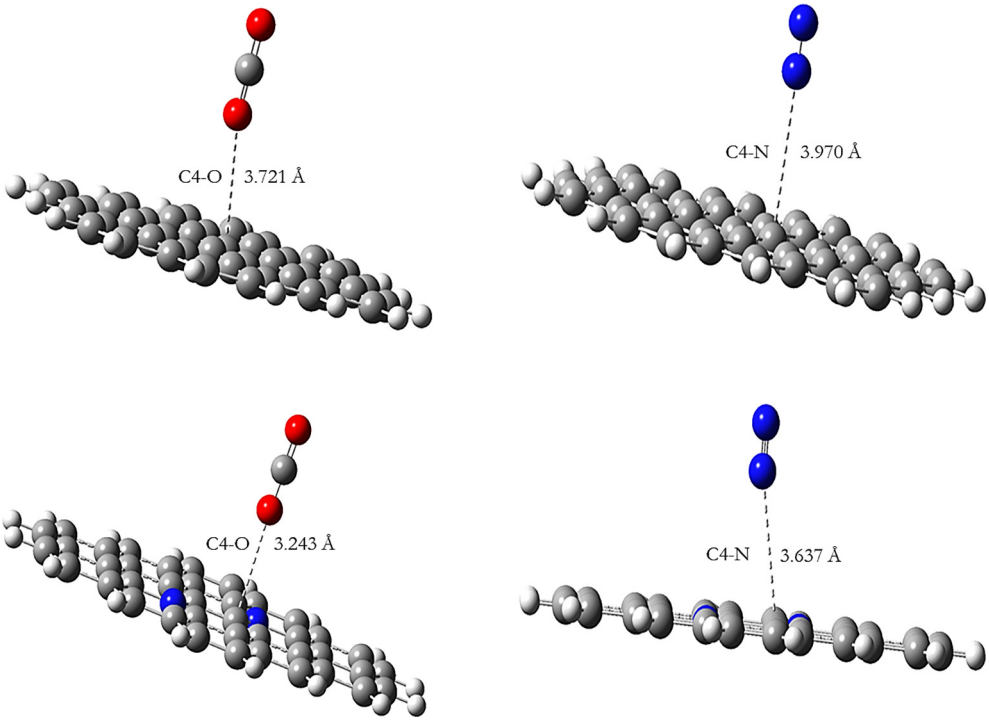

Fig. 11. Optimized structures of (a) SG-C (b) SG-CN in the adsorption of CO_2 and N_2 (from left to right) using B3LYP/6-31G (d).

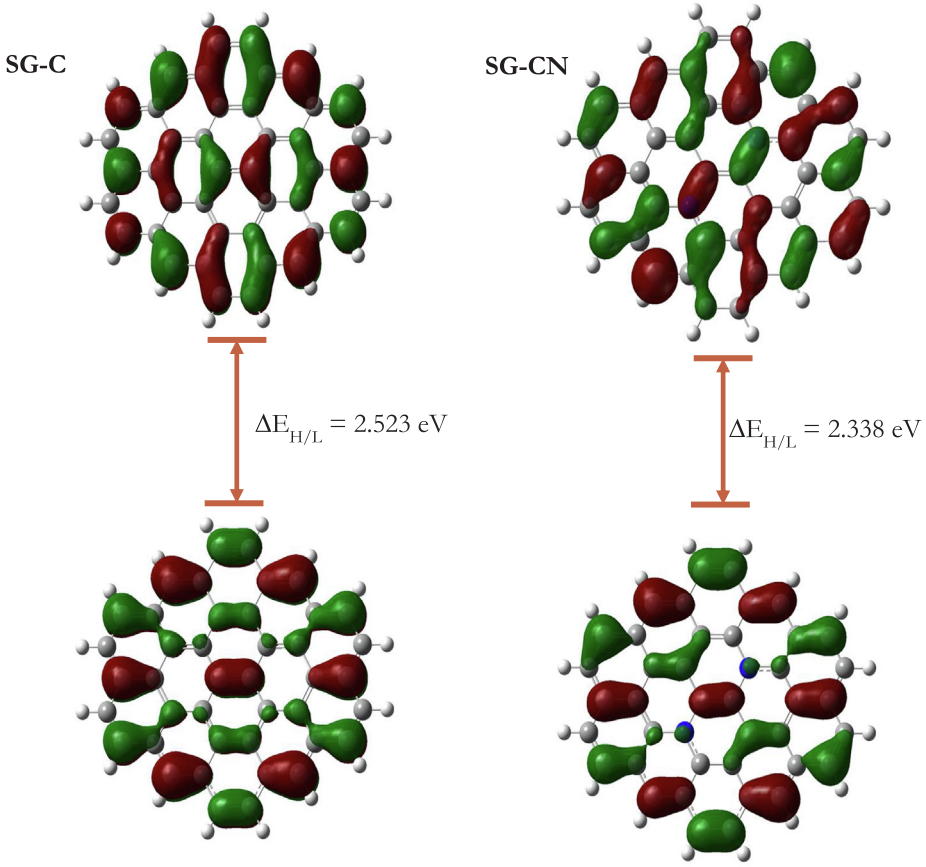

Fig. 12. Frontier orbital distribution of SG-C and SG-CN.

exhibited uneven size distribution and bulk morphology. The morphology also shows formation of flakes of less than 50 nm. The sizes of the SG-CN samples were also shown to be smaller than those of the parent carbon sample which may lead to increase in surface area [60]. The modified samples appear to be less dense and shows more porosity which is in accordance with the result obtained in the BET surface area analysis. Also, the cracks and crevices observed in the SEM micrograph of parent carbon (Fig. 6(a)) widened with melamine modification resulting in increased porosity. As explained above, porous structure must have been formed during the melamine pyrolysis step which occurred at high temperature. At this temperature (above 800 °C) more organic volatiles are evolved creating more spaces between the samples [61]. The Layer-like structure was also observed in the melamine modified samples confirming the polymerization of melamine. The quantitative amount of nitrogen was determined by EDX, and the nitrogen content increases in the sorbent by increasing the ratio of melamine incorporated in the pristine carbon as shown in Table 1. The nitrogen content in sorbent SG-CN(2) and SG-CN(3) are almost the same and one would have expected significant difference in both samples. This shows that further addition of nitrogen is not beneficial and directly correlated to the nitrogen content in the sorbent and again affecting the textural properties (surface area) by surface and void coverage.

3.2. Gas adsorption properties

3.2.1. Thermodynamic uptake capacity

Based on the high porosity and thermal stability observed, we sought to study the thermodynamic gas adsorption properties of the synthesized materials. Accordingly, low-pressure, single-component gas adsorption isotherms for CO_2 and N_2 were measured on pristine and newly synthesized materials at 298 K up to 760 Torr as shown in Fig. 7. All the modified carbon adsorbents show high CO_2 uptake capacities compared to the pristine material as summarized in table 2. The superiority showed by the modified materials can be attributed to strong reactivity between CO_2 and amine groups present on the modified materials [61,62]. Different explanation has been provided for this occurrence. Vidal et al. [63], explained this interaction using Nitrogen doped nanohoops where the larger the number of nitrogen atoms in the nanohoops, the richer the electron density that ensures interaction with CO_2 molecule. The concept of Lewis acid and Lewis base has also been used to explain this phenomenon. Interestingly, the SG-CN prepared using 1:2 (AC: Melamine) revealed the highest CO_2 uptake capacity of 3.34 mmol g^{-1} (74.75 $cm^3 g^{-1}$) at 298 K and 760 Torr. It is important to note that this adsorbent has the highest surface area and pore volume of all the modified carbon material investigated in this study. While the presence of nitrogen atom influences CO_2 uptake, the result obtained also shows that textural properties such as surface area and pore volume also contribute to CO_2 adsorption using N-containing adsorbents, a trend that has been reported by other authors. It also contributes to the assertion that the adsorption of CO_2 to our materials may be partly due to physisorption.

3.2.2. Sorbent selectivity to CO_2 in the presence of N_2

To understand the effect of N_2 in the adsorption of CO_2 from the same system and hence the selectivity of these materials, both the pristine and modified adsorbents were evaluated for N_2 capture. The N_2 uptake capacities under the same experimental conditions (298 K and 760 Torr) were low. As depicted in Fig. 8, SG-CN(2) displays a much higher CO_2 uptake at 298 K when compared to the N_2 uptake. This observation is indicative of stronger nitrogen–CO_2 interactions (i.e. higher affinity), which lends credence to the potential of this material to serve as an adsorbent for selective CO_2 capture from flue gas. The CO_2 uptake demonstrated by our materials was also compared with similar materials (carbon nitride or nitrogen doped carbon materials), conventional adsorbents and other highly ranked materials that have been reported (Table 3). Compared to established materials with strong binding potentials, our materials performed excellently at ambient conditions. As shown in Table 3, SG-CN(2) performed better than both zeolitic and other similar carbon–nitrogen based materials with different precursors. In addition to the outstanding performance of our material, the use of readily available precursors and sustainable feedstock in its synthesis lends superiority to the adoption of this material for CO_2 adsorption. Hence-forth, SG-CN(2) was studied for regenerative potentials.

3.2.3. Coverage-dependent enthalpy of adsorption

Due to the thermodynamic gas adsorption measurement results, we were encouraged to pursue a deeper understanding of SG-CN relationship with CO_2. Accordingly, the coverage-dependent enthalpy of adsorption (isosteric heat of adsorption, Qst) for CO_2 was estimated by fitting the isotherms collected at 298 K and 313 K [61] with a virial-type expansion equation. The resulting initial Qst value for pristine AC was calculated to be 39.50 kJ mol^{-1}. The resulting initial Qst value for prepared nitrogen-modified carbon was calculated to be 32.61 kJ mol^{-1}, which quantifiably demonstrates the material's physisorption affinity to CO_2 (Fig. 9). It is noted that the Qst remained relatively constant, thus, reflecting the homogeneous binding strengths over multiple sites at low coverage. The Qst value is moderately close for physisorption-driven materials as compared to related materials: BILP-1 (26.5 kJ mol^{-1}) [64], Azo-COP-1 (29.3 kJ mol^{-1}) [65], KFUPM-1 (34 kJ mol^{-1}) [66], SNW-1 (35 kJ mol^{-1}) and NENP-1 (37.5 kJmol^{-1}) [67]. To ensure balance between reversibility and selectivity of CO_2, Qst values between 30 and 50 kJ/mol is desired and has been reported by different literatures as the optimum value for gas adsorption. As such the Qst value obtained for the SG-CN materials reflect the reversible CO_2 binding nature of nitrogen containing adsorbents [61,68]. The values are also similar to those that have previously been reported.

3.3. DFT computational results

Unlike the experimental section above where CO_2 adsorption potentials of four adsorbents were evaluated, this part of the study is limited to understanding the effect of nitrogen modification on the CO_2 adsorption. As such, adsorption potentials of non-modified carbon material (SG-C) and nitrogen modified carbon material (SG-CN) were compared. The optimized structure of the coronene model used is shown in Fig. 10(a). The carbon atoms in this structure were saturated with hydrogen atoms. On the other hand, the model that depicts nitrogen modified carbon material is shown in Fig. 10(b) where two carbon atoms were substituted for nitrogen atoms. CO_2 molecule, after optimization, was placed above the central coronene structure and the effect of nitrogen modification on interaction between adsorbent and adsorbate was studied. Changes to bond lengths, bond angles and the binding distance between the adsorbent and the adsorbate as well as the adsorption energies were evaluated as illustrated in Table 4. In addition, the same properties were evaluated when the adsorption of N_2 gas to the adsorbents were considered instead of CO_2 gas.

As shown, very little change was observed in the bond lengths of the coronene structures before and after the addition of the gases. The bond lengths of SG-C, C1-C2-C3-C4-C5-C6, are 1.421, 1.429, 1.412, 1.429 and 1.421. The bond angles were also unchanged in both pre-adsorbed and adsorbed coronene structure. The binding distance between CO_2 and SG-CN was shorter (3.243 Å) compared to that between CO_2 and SG-C (3.721 Å). This demonstrates the propensity of nitrogen modified carbon to adsorb CO_2 gas more than non-modified carbon. Thus, it shows CO_2 molecule has a strong interaction to the nitrogen atoms in the carbon material. Also, the binding distances between the adsorbents and the gases (CO_2 and N_2) were compared (Fig. 11). In each case, the distance between CO_2 and both pristine and the modified carbon material was closer than that between N_2 and the carbon materials. This typifies the selectivity and higher affinity of the adsorbents towards

CO_2 adsorption compared to N_2.

In accordance with the order observed in the binding distances, the adsorption energy of SG-GC was also stronger than that of SG-C. The adsorption energy obtained in the adsorption of CO_2 to SG-CN was −51.86 Kcal/mol compared to that obtained for SG-C −48.92 Kcal/mol. The negative sign indicates that the adsorption is exergonic. The superiority demonstrated by the modified carbon material can also be understood in terms of the frontier orbital energy gap of the material before adsorption. The energy gap is the difference in the lowest unoccupied molecular orbital (LUMO) and highest occupied molecular orbital (HOMO). As shown in Fig. 12, SG-CN has a narrower energy gap and consequently a superior charge transfer characteristic. This explains the reason why SG-CN shows higher adsorption potential compared to SG-C. The narrow energy gap of SG-CN is an indication of the reactivity of this material and the ease at which electrons can move between the two-energy levels and influence CO_2 adsorption. In addition, SG-CN exhibited lower global hardness, η of 1.169 eV relative to SG-C with 1.262 eV which further explains the reactivity of the adsorbent towards CO_2 gas in accordance with the hard-soft acid-base principle [75]. The result obtained from the DFT calculation revealed that functionalization of SG-C led to enhancement in charge transfer capability and a decrease in hardness and provided a rationale on the dominance of SG-CN over SG-C; in conformation with experimental results

4. Conclusions

In summary, nitrogen-modified carbon CO_2 adsorbents were synthesized using low-cost and sustainable source of carbon (sugarcane bagasse) with solid state impregnation using melamine. The effect of increased amine functionalization on both the textural properties and the sorption capacity was also investigated. All the nitrogen-modified adsorbents were found to have higher CO_2 uptake compared with the pristine carbon material. Apparently, amine functionalization contributed to the increased sorption, an observation that was attributed to the affinity between nitrogen and CO_2. The nitrogen-modified carbon with an intermediate nitrogen content was found to have the highest surface area and micropore volume and therefore the highest CO_2 capture. This material also showed better sorption capacities compared to recently reported and conventional materials of high binding properties. These sorbents were also CO_2/N_2 selective and exhibited regenerative capabilities. Insights into the effect of nitrogen functionalization on carbon and its role in CO2 adsorption were revealed using DFT calculations. Considering the high efficiency, low-cost feedstock and environmentally benign source of carbon used, the synthesis and application of the material reported in this study is a significant contribution to sustainable CO_2 capture.

Declaration of Competing Interest

The authors declare that they have no known competing financial interests or personal relationships that could have appeared to influence the work reported in this paper.

Acknowledgment

The authors acknowledged the support provided by Saudi Aramco for funding this work through King Fahd University of Petroleum and Minerals, under project # CHEM2433.

References

[1] D.Y.C. Leung, G. Caramanna, M.M. Maroto-Valer, An overview of current status of carbon dioxide capture and storage technologies, Renew. Sustain. Energy Rev. 39 (2014) 426–443, https://doi.org/10.1016/j.rser.2014.07.093.

[2] P. Nejat, F. Jomehzadeh, M.M. Taheri, M. Gohari, M.Z.Abd Majid, A global review of energy consumption, CO2 emissions and policy in the residential sector (with an overview of the top ten CO2 emitting countries), Renew. Sustain. Energy Rev. 43 (2015) 843–862, https://doi.org/10.1016/J.RSER.2014.11.066.

[3] A.S. Alshehry, M. Belloumi, Energy consumption, carbon dioxide emissions and economic growth: the case of Saudi Arabia, Renew. Sustain. Energy Rev. 41 (2015) 237–247, https://doi.org/10.1016/j.rser.2014.08.004.

[4] S. Wang, X. Liu, C. Zhou, J. Hu, J. Ou, Examining the impacts of socioeconomic factors, urban form, and transportation networks on CO2 emissions in China's megacities, Appl. Energy 185 (2017) 189–200, https://doi.org/10.1016/j.apenergy.2016.10.052.

[5] A.L. Yaumi, M.Z.A. Bakar, B.H. Hameed, Recent advances in functionalized composite solid materials for carbon dioxide capture, Energy 124 (2017) 461–480, https://doi.org/10.1016/j.energy.2017.02.053.

[6] R.-L. Tseng, F.-C. Wu, R.-S. Juang, Adsorption of CO2 at atmospheric pressure on activated carbons prepared from melamine-modified phenol–formaldehyde resins, Sep. Purif. Technol. 140 (2015) 53–60, https://doi.org/10.1016/j.seppur.2014.11.018.

[7] R.V. Siriwardane, M.-S. Shen, E.P. Fisher, J. Losch, Adsorption of CO $_2$ on zeolites at moderate temperatures, Energy Fuels 19 (2005) 1153–1159, https://doi.org/10.1021/ef040059h.

[8] H.V. Thang, L. Grajciar, P. Nachtigall, O. Bludský, C.O. Areán, E. Frýdová, R. Bulánek, Adsorption of CO2 in FAU zeolites: effect of zeolite composition, Catal. Today 227 (2014) 50–56, https://doi.org/10.1016/j.cattod.2013.10.036.

[9] R. Girimonte, B. Formisani, F. Testa, Adsorption of CO2 on a confined fluidized bed of pelletized 13X zeolite, Powder Technol. 311 (2017) 9–17, https://doi.org/10.1016/J.POWTEC.2017.01.033.

[10] J. Zhao, K. Xie, R. Singh, G. Xiao, Q. Gu, Q. Zhao, G. Li, P. Xiao, P.A. Webley, Li $^+$ /ZSM-25 zeolite as a CO_2 capture adsorbent with high selectivity and improved adsorption kinetics, showing CO_2- induced framework expansion, J. Phys. Chem. C. 122 (2018) 18933–18941, https://doi.org/10.1021/acs.jpcc.8b04152.

[11] L. Zhang, G. Wu, J. Jiang, Adsorption and diffusion of CO $_2$ and CH $_4$ in zeolitic imidazolate framework-8: effect of structural flexibility, J. Phys. Chem. C. 118 (2014) 8788–8794, https://doi.org/10.1021/jp500796e.

[12] A.M. Fracaroli, H. Furukawa, M. Suzuki, M. Dodd, S. Okajima, F. Gándara, J.A. Reimer, O.M. Yaghi, Metal-organic frameworks with precisely designed interior for carbon dioxide capture in the presence of water, J. Am. Chem. Soc. 136 (2014) 8863–8866, https://doi.org/10.1021/ja503296c.

[13] W.L. Queen, M.R. Hudson, E.D. Bloch, J.A. Mason, M.I. Gonzalez, J.S. Lee, D. Gygi, J.D. Howe, K. Lee, T.A. Darwish, M. James, V.K. Peterson, S.J. Teat, B. Smit, J.B. Neaton, J.R. Long, C.M. Brown, Comprehensive study of carbon dioxide adsorption in the metal–organic frameworks M $_2$ (dobdc) (M = Mg, Mn, Fe Co, Ni, Cu, Zn), Chem. Sci. 5 (2014) 4569–4581, https://doi.org/10.1039/C4SC02064B.

[14] R.L. Siegelman, T.M. McDonald, M.I. Gonzalez, J.D. Martell, P.J. Milner, J.A. Mason, A.H. Berger, A.S. Bhown, J.R. Long, Controlling cooperative CO $_2$ adsorption in diamine-appended Mg $_2$ (dobpdc) metal-organic frameworks, J. Am. Chem. Soc. 139 (2017) 10526–10538, https://doi.org/10.1021/jacs.7b05858.

[15] A. Arami-Niya, T.E. Rufford, Z. Zhu, Activated carbon monoliths with hierarchical pore structure from tar pitch and coal powder for the adsorption of CO 2, CH 4 and N 2, Carbon 103 (2016) 115–124, https://doi.org/10.1016/j.carbon.2016.02.098.

[16] A. Heidari, H. Younesi, A. Rashidi, A.A. Ghoreyshi, Evaluation of CO2 adsorption with eucalyptus wood based activated carbon modified by ammonia solution through heat treatment, Chem. Eng. J. 254 (2014) 503–513, https://doi.org/10.1016/j.cej.2014.06.004.

[17] A. Heidari, H. Younesi, A. Rashidi, A. Ghoreyshi, Adsorptive removal of CO2 on highly microporous activated carbons prepared from Eucalyptus camaldulensis wood: effect of chemical activation, J. Taiwan Inst. Chem. Eng. 45 (2014) 579–588, https://doi.org/10.1016/J.JTICE.2013.06.007.

[18] V.K. Singh, E. Anil Kumar, Measurement and analysis of adsorption isotherms of CO2 on activated carbon, Appl. Therm. Eng. 97 (2016) 77–86, https://doi.org/10.1016/j.applthermaleng.2015.10.052.

[19] S. Jin, K.-J. Ko, Y.-G. Song, K. Lee, C.-H. Lee, Fabrication and kinetic study of spherical MgO agglomerates via water-in-oil method for pre-combustion CO2 capture, Chem. Eng. J. 359 (2019) 285–297, https://doi.org/10.1016/J.CEJ.2018.11.131.

[20] Y. Hu, W. Liu, Y. Yang, M. Qu, H. Li, CO2 capture by Li4SiO4 sorbents and their applications: current developments and new trends, Chem. Eng. J. 359 (2019) 604–625, https://doi.org/10.1016/J.CEJ.2018.11.128.

[21] Y. Hu, M. Qu, H. Li, Y. Yang, J. Yang, W. Qu, W. Liu, Porous extruded-spheronized Li4SiO4 pellets for cyclic CO2 capture, Fuel 236 (2019) 1043–1049, https://doi.org/10.1016/J.FUEL.2018.09.072.

[22] H. Li, M. Qu, Y. Yang, Y. Hu, W. Liu, One-step synthesis of spherical CaO pellets via novel graphite-casting method for cyclic CO2 capture, Chem. Eng. J. 374 (2019) 619–625, https://doi.org/10.1016/J.CEJ.2019.05.214.

[23] Y. Belmabkhout, V. Guillerm, M. Eddaoudi, Low concentration CO 2 capture using physical adsorbents: are metal–organic frameworks becoming the new benchmark materials? Chem. Eng. J. 296 (2016) 386–397, https://doi.org/10.1016/j.cej.2016.03.124.

[24] L. Huang, M. He, B. Chen, Q. Cheng, B. Hu, Highly efficient magnetic nitrogen-doped porous carbon prepared by one-step carbonization strategy for Hg $^{2+}$ removal from water, ACS Appl. Mater. Interf. 9 (2017) 2550–2559, https://doi.org/10.1021/acsami.6b15106.

[25] Y. Shen, P. Zhao, Q. Shao, Porous silica and carbon derived materials from rice husk pyrolysis char, Micropor. Mesopor. Mater. 188 (2014) 46–76, https://doi.org/10.1016/j.micromeso.2014.01.005.

[26] L. Sun, K. Gong, Silicon-based materials from rice husks and their applications, Ind. Eng. Chem. Res. 40 (2001) 5861–5877, https://doi.org/10.1021/ie010284b.

[27] M. Olivares-Marín, M.M. Maroto-Valer, Development of adsorbents for CO2 capture from waste materials: a review, Greenhouse Gases Sci. Technol. 2 (2012) 20–35, https://doi.org/10.1002/ghg.45.

[28] L. Sim, W. Tan, K. Leong, M. Bashir, P. Saravanan, N. Surib, Mechanistic characteristics of surface modified organic semiconductor g-C3N4 nanotubes alloyed

with Titania, Materials 10 (2017) 28, https://doi.org/10.3390/ma10010028.
[29] H. Niu, Y. Wang, X. Zhang, Z. Meng, Y. Cai, Easy synthesis of surface-tunable carbon-encapsulated magnetic nanoparticles: adsorbents for selective isolation and preconcentration of organic pollutants, ACS Appl. Mater. Interfaces 4 (2012) 286–295, https://doi.org/10.1021/am201336n.
[30] E. Fagury Neto, R.H.G.A. Kiminami, Synthesis of silicon nitride by conventional and microwave carbothermal reduction and nitridation of rice hulls, Adv. Powder Technol. 25 (2014) 654–658, https://doi.org/10.1016/j.apt.2013.10.009.
[31] X. Niu, H. Zhao, C. Chen, M. Lan, Platinum nanoparticle-decorated carbon nanotube clusters on screen-printed gold nanofilm electrode for enhanced electrocatalytic reduction of hydrogen peroxide, Electrochim. Acta 65 (2012) 97–103, https://doi.org/10.1016/J.ELECTACTA.2012.01.030.
[32] C. Real, M.D. Alcalá, J.M. Criado, Synthesis of silicon nitride from carbothermal reduction of rice husks by the constant-rate-thermal-analysis (CRTA) method, J. Am. Ceram. Soc. 87 (2004) 75–78, https://doi.org/10.1111/j.1551-2916.2004.00075.x.
[33] X. Li, X. Pan, L. Yu, P. Ren, X. Wu, L. Sun, F. Jiao, X. Bao, Silicon carbide-derived carbon nanocomposite as a substitute for mercury in the catalytic hydrochlorination of acetylene, Nat. Commun. 5 (2014) 3688, https://doi.org/10.1038/ncomms4688.
[34] J. Zhao, T. Zhang, X. Di, J. Xu, J. Xu, F. Feng, J. NI, X. Li, Nitrogen-modified activated carbon supported bimetallic gold–cesium (i) as highly active and stable catalyst for the hydrochlorination of acetylene, RSC Adv. 5 (2015) 6925–6931, https://doi.org/10.1039/C4RA11654B.
[35] N.K. Gupta, B. Peng, G.L. Haller, E.E. Ember, J.A. Lercher, Nitrogen modified carbon nano-materials as stable catalysts for phosgene synthesis, ACS Catal. 6 (2016) 5843–5855, https://doi.org/10.1021/acscatal.6b01424.
[36] S.L. Candelaria, B.B. Garcia, D. Liu, G. Cao, Nitrogen modification of highly porous carbon for improved supercapacitor performance, J. Mater. Chem. 22 (2012) 9884, https://doi.org/10.1039/c2jm30923h.
[37] G. Liu, X. Li, J.-W. Lee, B.N. Popov, A review of the development of nitrogen-modified carbon-based catalysts for oxygen reduction at USC, Catal. Sci. Technol. 1 (2011) 207, https://doi.org/10.1039/c0cy00053a.
[38] H. Wei, J. Chen, N. Fu, H. Chen, H. Lin, S. Han, Biomass-derived nitrogen-doped porous carbon with superior capacitive performance and high CO2 capture capacity, Electrochim. Acta 266 (2018) 161–169, https://doi.org/10.1016/J.ELECTACTA.2017.12.192.
[39] K. Dennington, Roy, Todd Keith, and John Millam 2009. “GaussView, version 5.” Semichem Inc.: Shawnee Mission, No Title, (n.d.).
[40] M.J. Frisch, G.W. Trucks, H.B. Schlegel, G.E. Scuseria, M.A. Robb, J.R. Cheeseman, G. Scalmani, et al. Gaussian 09, Revision A. 02; Gaussian, Inc: Wallingford, CT, 2009.” There is no corresponding record for this reference. [Google Scholar], 2015, (n.d.).
[41] W. Dai, Y. Liu, W. Su, G. Hu, G. Deng, X. Hu, Preparation and CO_2 sorption of a high surface area activated carbon obtained from the KOH activation of finger citron residue, Adsorpt. Sci. Technol. 30 (2012) 183–191, https://doi.org/10.1260/0263-6174.30.2.183.
[42] R. Gong, J. Ye, W. Dai, X. Yan, J. Hu, X. Hu, S. Li, H. Huang, Adsorptive removal of methyl orange and methylene blue from aqueous solution with finger-citron-residue-based activated carbon, Ind. Eng. Chem. Res. 52 (2013) 14297–14303, https://doi.org/10.1021/ie402138w.
[43] A. Kongnoo, P. Intharapat, P. Worathanakul, C. Phalakornkule, Diethanolamine impregnated palm shell activated carbon for CO2 adsorption at elevated temperatures, J. Environ. Chem. Eng. 4 (2016) 73–81, https://doi.org/10.1016/J.JECE.2015.11.015.
[44] R.F.P. Moreira, H. José, A. Rodrigues, Modification of pore size in activated carbon by polymer deposition and its effects on molecular sieve selectivity, Carbon 39 (2001) 2269–2276, https://doi.org/10.1016/S0008-6223(01)00046-X.
[45] S. Yang, Y. Gong, J. Zhang, L. Zhan, L. Ma, Z. Fang, R. Vajtai, X. Wang, P.M. Ajayan, Exfoliated graphitic carbon nitride nanosheets as efficient catalysts for hydrogen evolution under visible light, Adv. Mater. 25 (2013) 2452–2456, https://doi.org/10.1002/adma.201204453.
[46] K. Ramesh, M. Prashantha, N.K. Reddy, E.S.R. Gopal, Synthesis of nano structured carbon nitride by pyrolysis assisted chemical vapour deposition, Integr. Ferroelectr. 117 (2010) 40–48, https://doi.org/10.1080/10584587.2010.489421.
[47] A. Vinu, K. Ariga, T. Mori, T. Nakanishi, S. Hishita, D. Golberg, Y. Bando, Preparation and characterization of well-ordered hexagonal mesoporous carbon nitride, Adv. Mater. 17 (2005) 1648–1652, https://doi.org/10.1002/adma.200401643.
[48] Y. Li, G. Wang, T. Wei, Z. Fan, P. Yan, Nitrogen and sulfur co-doped porous carbon nanosheets derived from willow catkin for supercapacitors, Nano Energy 19 (2016) 165–175, https://doi.org/10.1016/J.NANOEN.2015.10.038.
[49] Y.-Q. Zhao, M. Lu, P.-Y. Tao, Y.-J. Zhang, X.-T. Gong, Z. Yang, G.-Q. Zhang, H.-L. Li, Hierarchically porous and heteroatom doped carbon derived from tobacco rods for supercapacitors, J. Power Sour. 307 (2016) 391–400, https://doi.org/10.1016/J.JPOWSOUR.2016.01.020.
[50] S.A. Ganiyu, K. Alhooshani, K.O. Sulaiman, M. Qamaruddin, I.A. Bakare, A. Tanimu, T.A. Saleh, Influence of aluminium impregnation on activated carbon for enhanced desulfurization of DBT at ambient temperature: role of surface acidity and textural properties, Chem. Eng. J. 303 (2016) 489–500, https://doi.org/10.1016/J.CEJ.2016.06.005.
[51] L.G. Bulusheva, A.V. Okotrub, I.A. Kinloch, I.P. Asanov, A.G. Kurenya, A.G. Kudashov, X. Chen, H. Song, Effect of nitrogen doping on Raman spectra of multi-walled carbon nanotubes, Physica Stat. Solidi (B) 245 (2008) 1971–1974, https://doi.org/10.1002/pssb.200879592.
[52] H. Ou, L. Lin, Y. Zheng, P. Yang, Y. Fang, X. Wang, Tri- *s* -triazine-based crystalline carbon nitride nanosheets for an improved hydrogen evolution, Adv. Mater. 29 (2017) 1700008, https://doi.org/10.1002/adma.201700008.
[53] Q. Su, X. Yao, W. Cheng, S. Zhang, Boron-doped melamine-derived carbon nitrides tailored by ionic liquids for catalytic conversion of CO_2 into cyclic carbonates, Green Chem. 19 (2017) 2957–2965, https://doi.org/10.1039/C7GC00279C.
[54] Q. Zhuang, L. Sun, Y. Ni, One-step synthesis of graphitic carbon nitride nanosheets with the help of melamine and its application for fluorescence detection of mercuric ions, Talanta 164 (2017) 458–462, https://doi.org/10.1016/J.TALANTA.2016.12.004.
[55] Y. Zhang, S. Zong, C. Cheng, J. Shi, X. Guan, Y. Lu, L. Guo, One-pot annealing preparation of Na-doped graphitic carbon nitride from melamine and organometallic sodium salt for enhanced photocatalytic H2 evolution, Int. J. Hydrogen Energy 43 (2018) 13953–13961, https://doi.org/10.1016/J.IJHYDENE.2018.04.042.
[56] A. Hatamie, F. Marahel, A. Sharifat, Green synthesis of graphitic carbon nitride nanosheet (g-C3N4) and using it as a label-free fluorosensor for detection of metronidazole via quenching of the fluorescence, Talanta 176 (2018) 518–525, https://doi.org/10.1016/J.TALANTA.2017.08.059.
[57] F. Hou, Y. Li, Y. Gao, S. Hu, B. Wu, H. Bao, H. Wang, B. Jiang, Non-metal boron modified carbon nitride tube with enhanced visible light-driven photocatalytic performance, Mater. Res. Bull. 110 (2019) 18–23, https://doi.org/10.1016/J.MATERRESBULL.2018.10.009.
[58] Y. Zhang, T. Mori, J. Ye, M. Antonietti, Phosphorus-doped carbon nitride solid: enhanced electrical conductivity and photocurrent generation, J. Am. Chem. Soc. 132 (2010) 6294–6295, https://doi.org/10.1021/ja101749y.
[59] G.-P. Hao, W.-C. Li, D. Qian, A.-H. Lu, Rapid synthesis of nitrogen-doped porous carbon monolith for CO_2 capture, Adv. Mater. 22 (2010) 853–857, https://doi.org/10.1002/adma.200903765.
[60] H. Ma, Z. Shi, Q. Li, S. Li, Preparation of graphitic carbon nitride with large specific surface area and outstanding N2 photofixation ability via a dissolve-regrowth process, J. Phys. Chem. Solids 99 (2016) 51–58, https://doi.org/10.1016/J.JPCS.2016.08.008.
[61] D.J. Babu, M. Bruns, R. Schneider, D. Gerthsen, J.J. Schneider, Understanding the influence of N-doping on the CO_2 adsorption characteristics in carbon nanomaterials, J. Phys. Chem. C 121 (2017) 616–626, https://doi.org/10.1021/acs.jpcc.6b11686.
[62] D. Li, Y. Chen, M. Zheng, H. Zhao, Y. Zhao, Z. Sun, Hierarchically structured porous nitrogen-doped carbon for highly selective CO_2 capture, ACS Sustain. Chem. Eng. 4 (2016) 298–304, https://doi.org/10.1021/acssuschemeng.5b01230.
[63] Á. Vidal Vidal, C.S. López, O. Nieto Faza, Nitrogen doped nanohoops as promising CO_2 capturing devices, PCCP 20 (2018) 8607–8615, https://doi.org/10.1039/C7CP08498F.
[64] M.G. Rabbani, H.M. El-Kaderi, Template-free synthesis of a highly porous benzimidazole-linked polymer for CO_2 capture and H_2 storage, Chem. Mater. 23 (2011) 1650–1653, https://doi.org/10.1021/cm200411p.
[65] H.A. Patel, S. Hyun Je, J. Park, D.P. Chen, Y. Jung, C.T. Yavuz, A. Coskun, Unprecedented high-temperature CO2 selectivity in N2-phobic nanoporous covalent organic polymers, Nat. Commun. 4 (2013) 1357, https://doi.org/10.1038/ncomms2359.
[66] M.M. Abdelnaby, A.M. Alloush, N.A.A. Qasem, B.A. Al-Maythalony, R.B. Mansour, K.E. Cordova, O.C.S. Al, Hamouz, Carbon dioxide capture in the presence of water by an amine-based crosslinked porous polymer, J. Mater. Chem. A 6 (2018) 6455–6462, https://doi.org/10.1039/C8TA00012C.
[67] M. Chaudhary, R. Muhammad, C.N. Ramachandran, P. Mohanty, Nitrogen amelioration-driven carbon dioxide capture by nanoporous polytriazine, Langmuir 35 (2019) 4893–4901, https://doi.org/10.1021/acs.langmuir.9b00643.
[68] L. Yang, G. Chang, D. Wang, High and selective carbon dioxide capture in nitrogen-containing aerogels via synergistic effects of electrostatic in-plane and dispersive π–π-stacking interactions, ACS Appl. Mater. Interfaces 9 (2017) 15213–15218, https://doi.org/10.1021/acsami.7b02077.
[69] M.R. Mello, D. Phanon, G.Q. Silveira, P.L. Llewellyn, C.M. Ronconi, Amine-modified MCM-41 mesoporous silica for carbon dioxide capture, Microporous Mesoporous Mater. 143 (2011) 174–179, https://doi.org/10.1016/J.MICROMESO.2011.02.022.
[70] J. Park, N.F. Attia, M. Jung, M.E. Lee, K. Lee, J. Chung, H. Oh, Sustainable nanoporous carbon for CO2, CH4, N2, H2 adsorption and CO2/CH4 and CO2/N2 separation, Energy 158 (2018) 9–16, https://doi.org/10.1016/J.ENERGY.2018.06.010.
[71] K. Sim, N. Lee, J. Kim, E.-B. Cho, C. Gunathilake, M. Jaroniec, CO_2 adsorption on amine-functionalized periodic mesoporous benzenesilicas, ACS Appl. Mater. Interfaces 7 (2015) 6792–6802, https://doi.org/10.1021/acsami.5b00306.
[72] Q. Li, J. Yang, D. Feng, Z. Wu, Q. Wu, S.S. Park, C.-S. Ha, D. Zhao, Facile synthesis of porous carbon nitride spheres with hierarchical three-dimensional mesostructures for CO2 capture, Nano Res. 3 (2010) 632–642, https://doi.org/10.1007/s12274-010-0023-7.
[73] B. Liu, L. Ye, R. Wang, J. Yang, Y. Zhang, R. Guan, L. Tian, X. Chen, Phosphorus-doped graphitic carbon nitride nanotubes with amino-rich surface for efficient CO_2 capture, enhanced photocatalytic activity, and product selectivity, ACS Appl. Mater. Interf. 10 (2018) 4001–4009, https://doi.org/10.1021/acsami.7b17503.
[74] Q.-F. Deng, L. Liu, X.-Z. Lin, G. Du, Y. Liu, Z.-Y. Yuan, Synthesis and CO2 capture properties of mesoporous carbon nitride materials, Chem. Eng. J. 203 (2012) 63–70, https://doi.org/10.1016/J.CEJ.2012.06.124.
[75] I. Abdulazeez, C. Basheer, A.A. Al-Saadi, A selective detection approach for copper (ii) ions using a hydrazone-based colorimetric sensor: spectroscopic and DFT study, RSC Adv. 8 (2018) 39983–39991, https://doi.org/10.1039/C8RA08807A.